Electronic Supplementary Material (ESI) for Materials Chemistry Frontiers.

Supporting Information

An advanced hybrid supercapacitor constructed from rugby-ball-like $NiCo_2Se_4$ yolk-shell nanostructures

Bahareh Ameri, Akbar Mohammadi Zardkhoshoui and Saied Saeed Hosseiny Davarani* Department of Chemistry, Shahid Beheshti University, G. C., 1983963113, Evin, Tehran, Iran. Corresponding author: *Tel: +98 21 22431661; Fax: +98 21 22431661; E-mail: ss-hosseiny@sbu.ac.ir (S.S.H. Davarani)

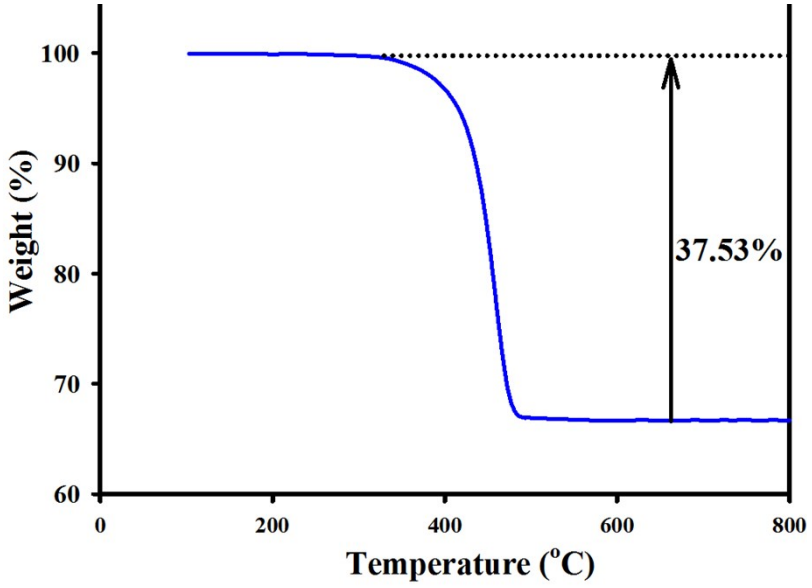

Fig S1. Thermal gravimetric analysis (TGA) of the $NiCO_3$@$CoCO_3$ precursor with the temperature ramp of 5 °C/min under air flow.

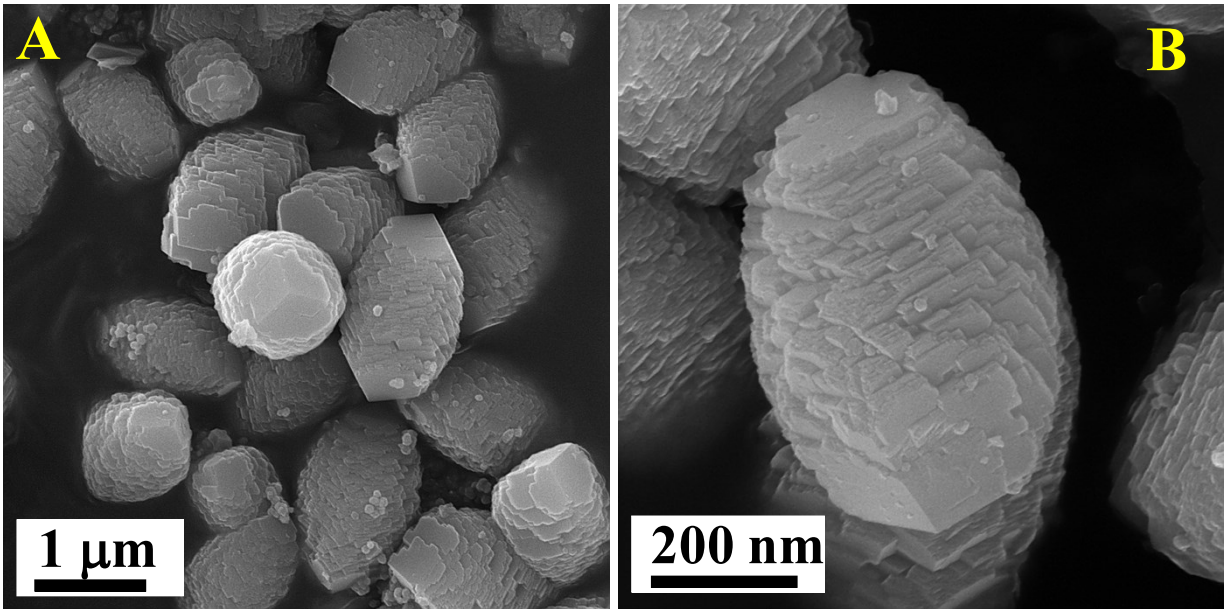

Fig S2. (A and B) FE-SEM images of the $NiCO_3$@$CoCO_3$ sample.

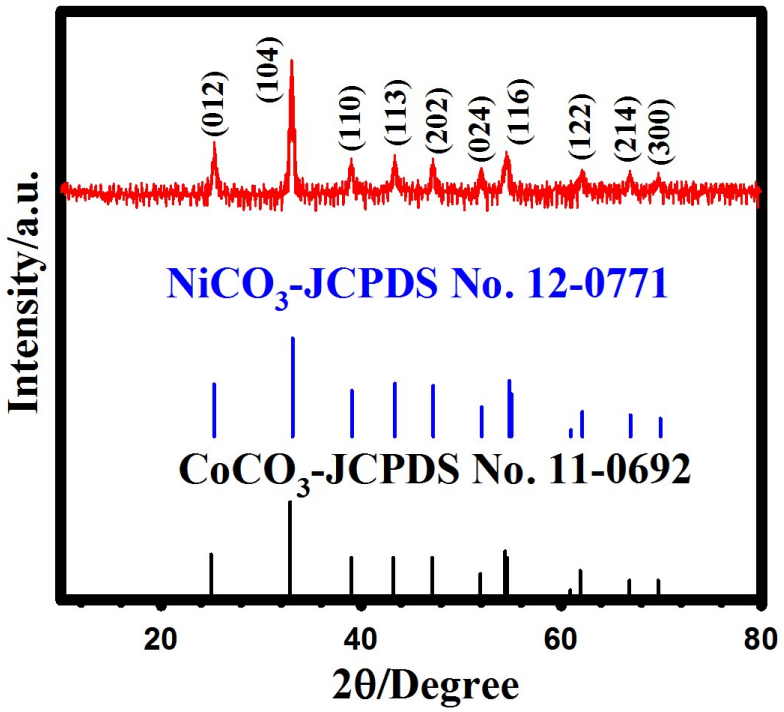

Fig S3. XRD pattern of the $NiCO_3$@$CoCO_3$ sample.

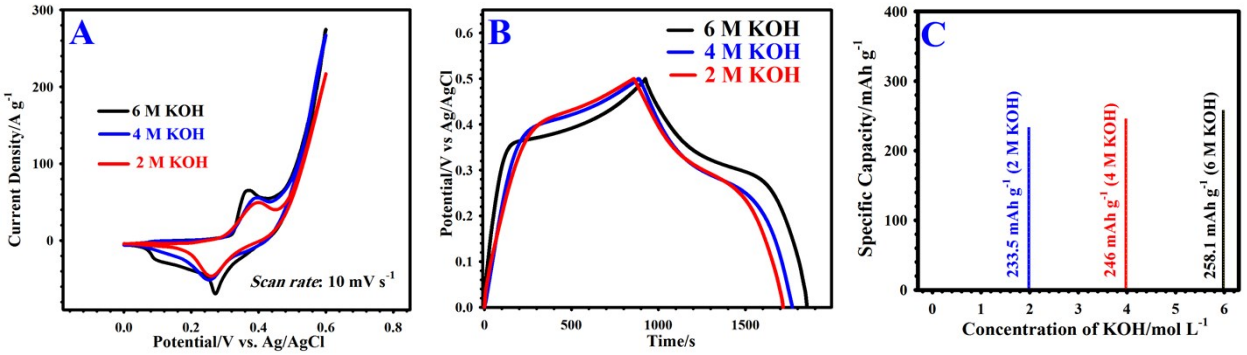

Fig S4. (A) CV profiles of the RB-NCS electrode at 10 mV/s in several concentration of KOH electrolyte. (B) GCD plots of the RB-NCS electrode at 1 A/g in various concentration of KOH electrolyte. (C) The specific capacity values of the RB-NCS electrode in several concentration of KOH electrolyte at 1 A/g.

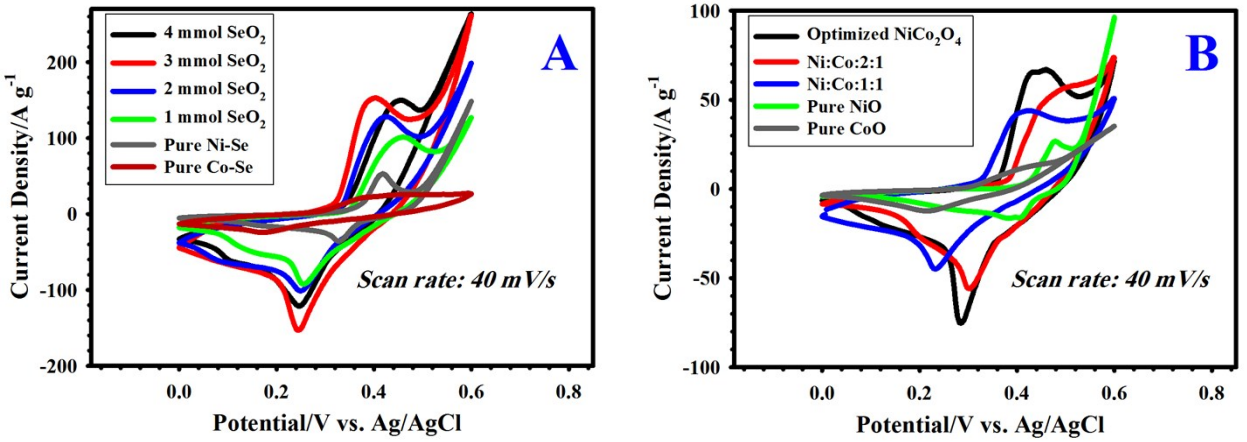

Fig S5. (A) CV curves of the Ni-Co-selenide electrodes at 40 mV/s. (B) CV curves of the Ni-Co-oxide electrodes at 40 mV/s.

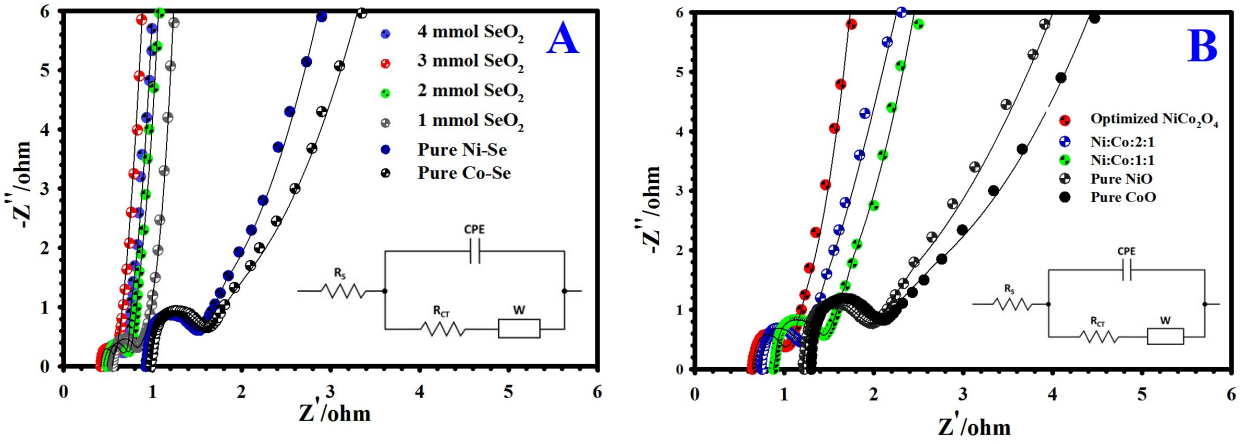

Fig S6. (A) EIS plots of the Ni-Co-selenide electrodes. (B) EIS plots of the Ni-Co-oxide electrodes.

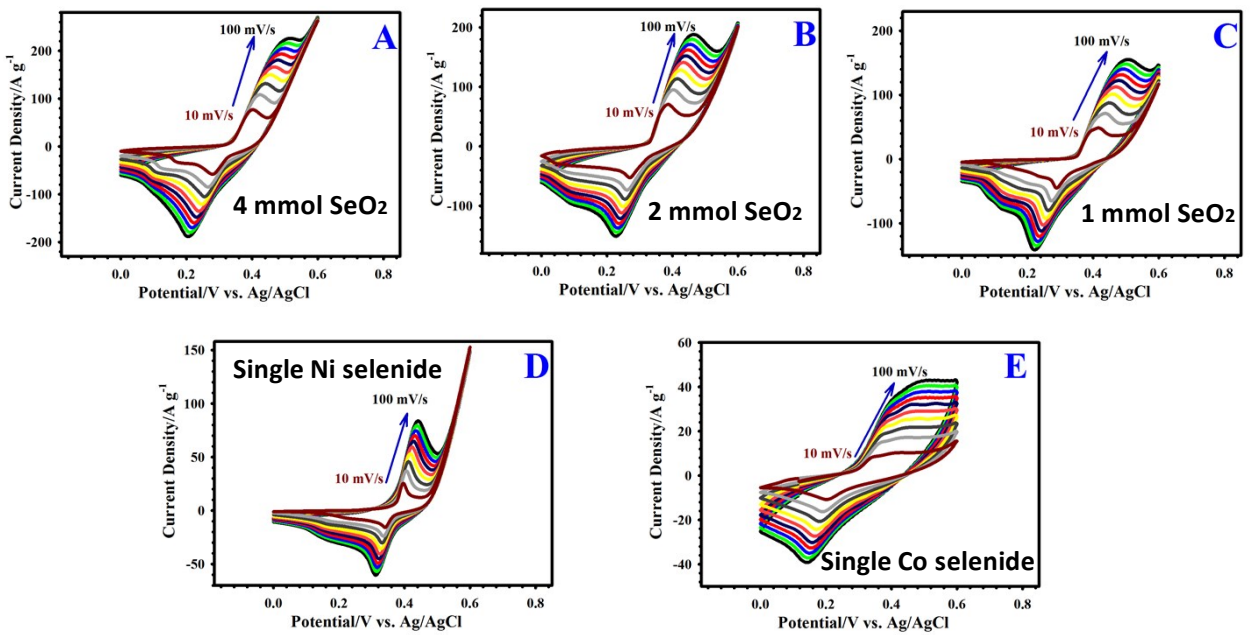

Fig S7. (A-E) CV curves of the Ni-Co-selenide electrodes at various scan rates.

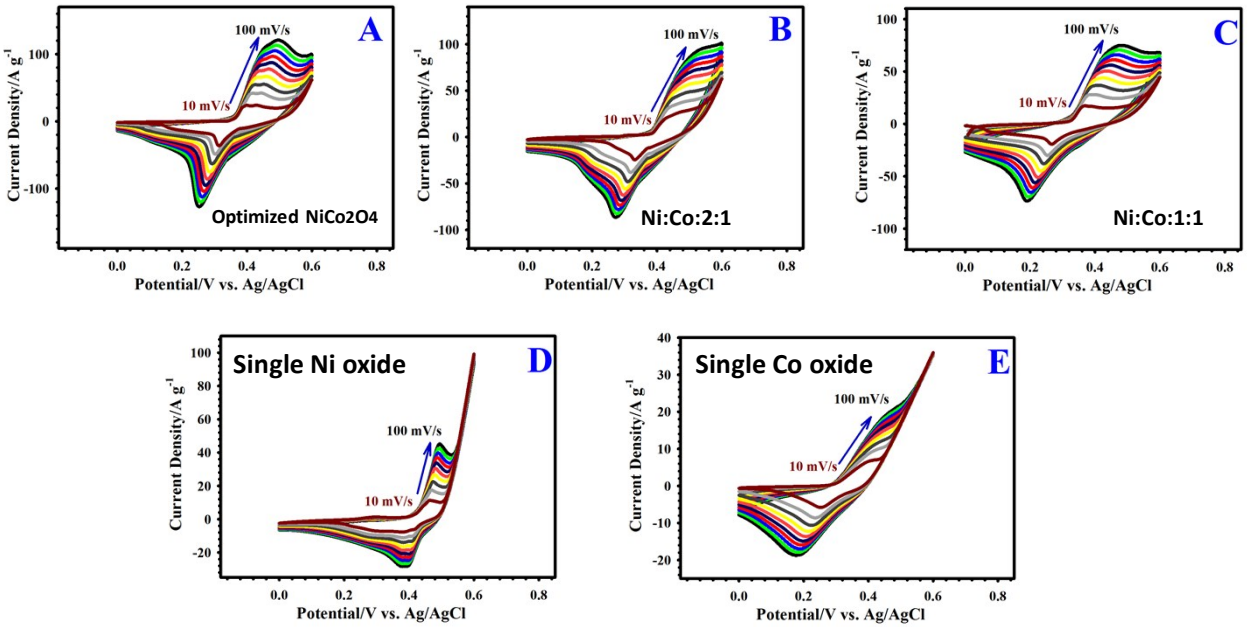

Fig S8. (A-E) CV curves of the Ni-Co-oxide electrodes at various scan rates.

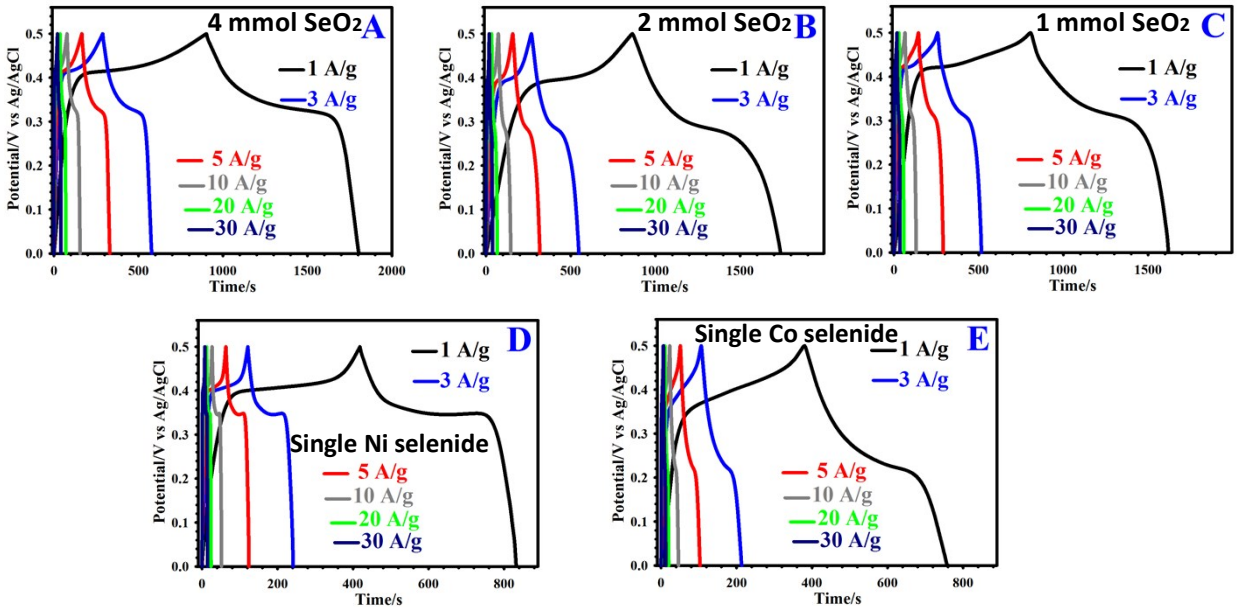

Fig S9. (A-E) GCD curves of the Ni-Co-selenide electrodes at various current densities.

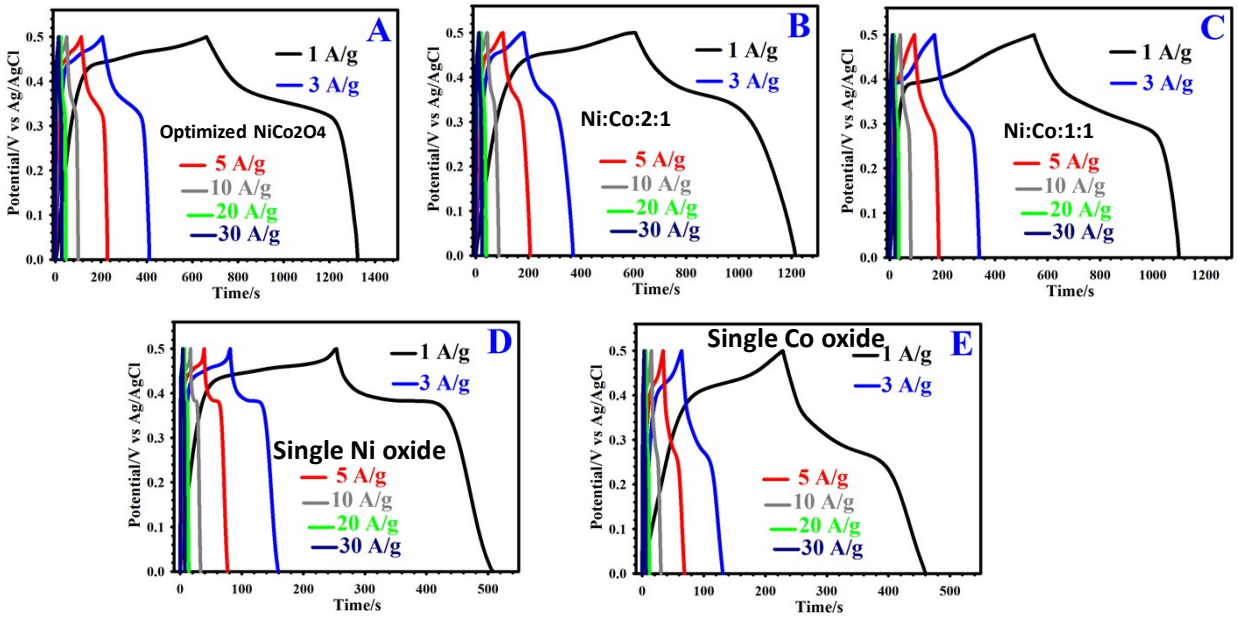

Fig S10. (A-E) GCD curves of the Ni-Co-oxide electrodes at various current densities.

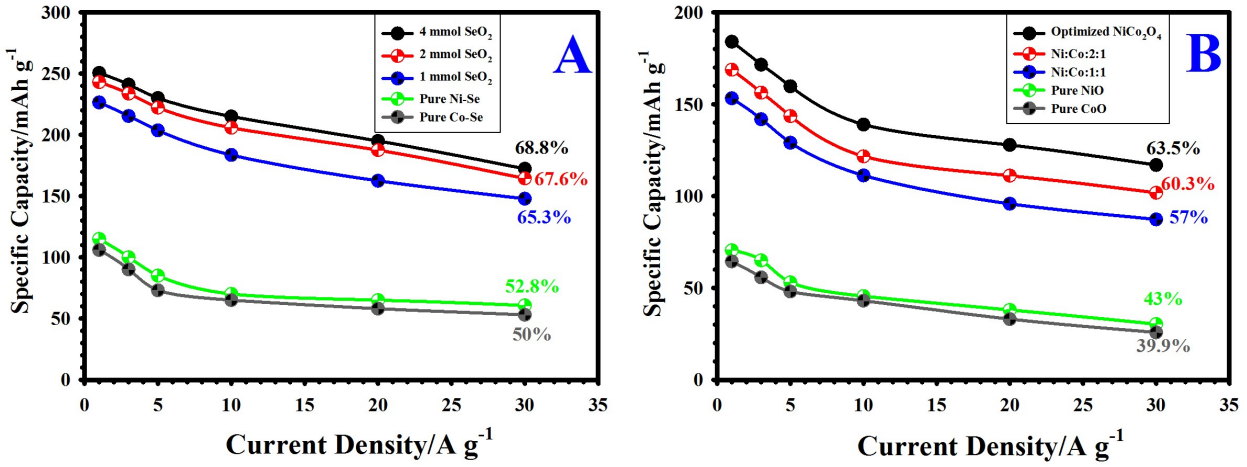

Fig S11. (A) Rate capability of the Ni-Co-selenide electrodes. (B) Rate capability of the Ni-Co-oxide electrodes.

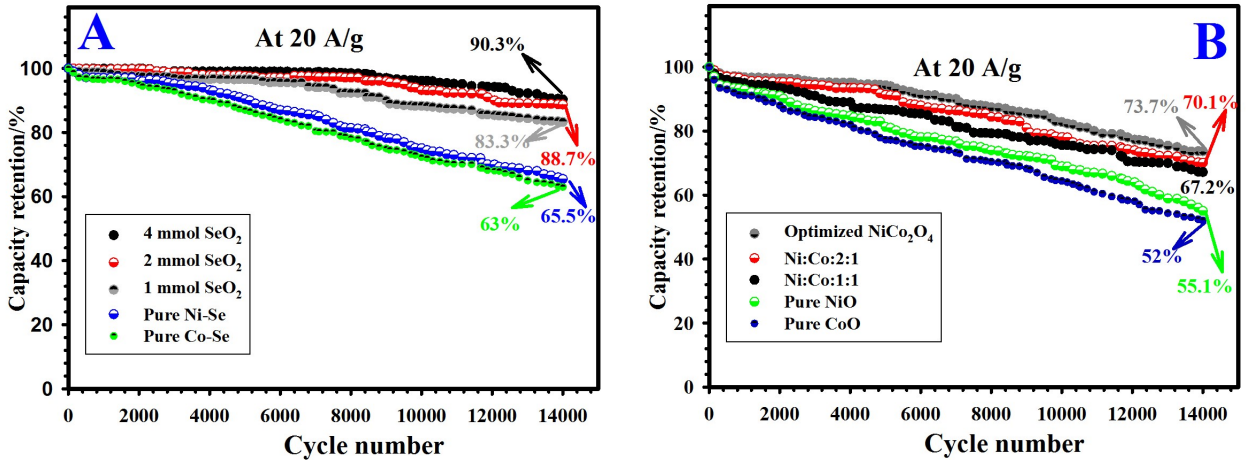

Fig S12. (A) Cyclic performance of the Ni-Co-selenide electrodes. (B) Cyclic performance of the Ni-Co-oxide electrodes.

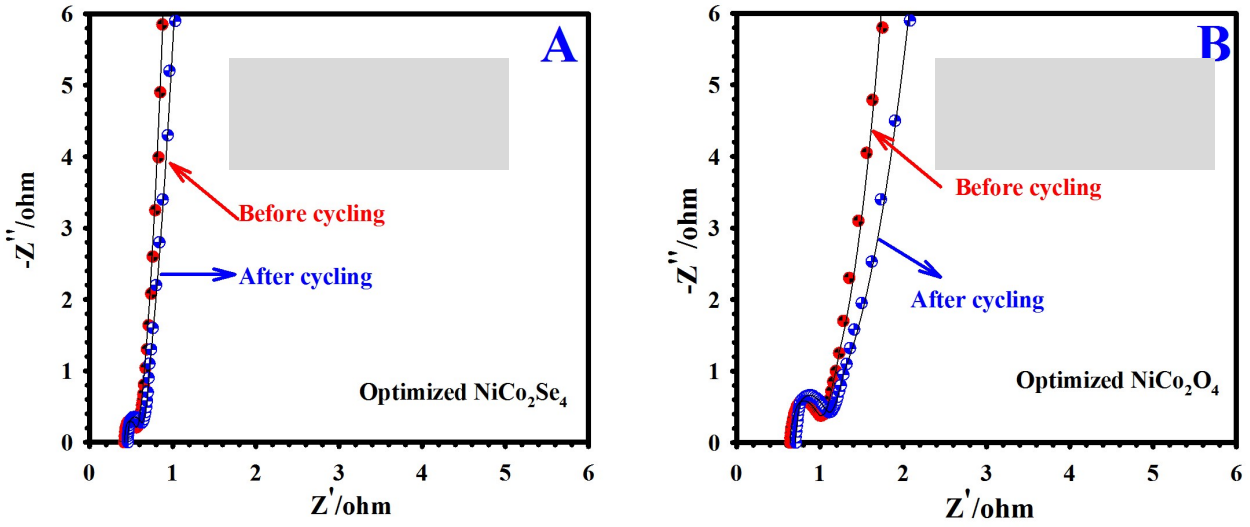

Fig S13. (A) EIS plots of the RB-NCS electrode before and after longevity test. (B) EIS plots of the RB-NCO electrode before and after longevity test.

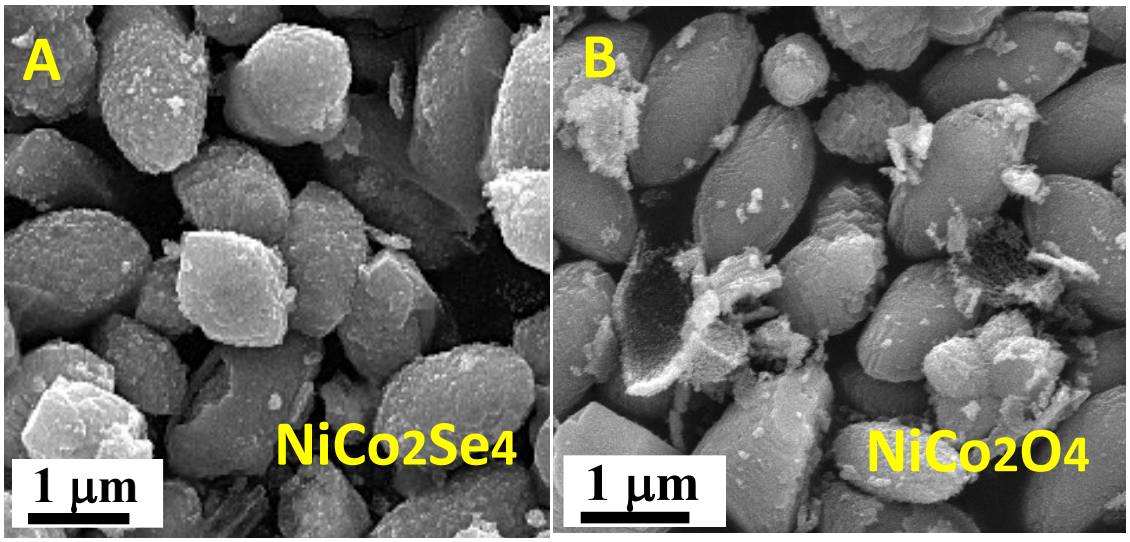

Fig S14. (A) FE-SEM image of the RB-NCS sample after longevity test. (B) FE-SEM image of the RB-NCO sample after longevity test.

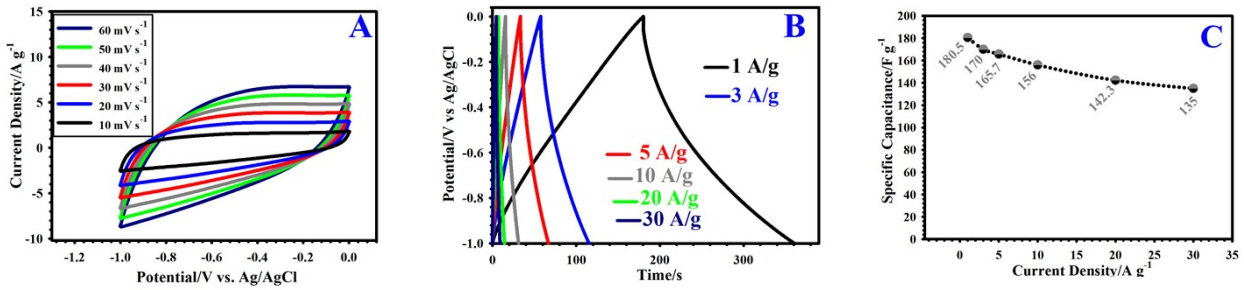

Fig S15. (A) CV curves of the AC-based electrode at various sweep speeds of 10-60 mV/s. (B) GCD curves of the AC-based electrode at various current densities of 1-30 A/g. (C) Specific capacity vs. current density of AC-based electrode.

Table S1. Comparison of the electrochemical performance of the RB-NCS-based electrode in three electrode systems with other previously reported electrodes.

Composition	Capacity (mAh g^{-1})	Cycles, retention	Rate capability	Reference
$CoSe_2$/NC	120.2 mAh g^{-1} at 1 A g^{-1}	10000, 92% (3 E)	61.2% at 20 A g^{-1}	1
(Ni, Co)Se_2	106 mAh g^{-1} at 1 A g^{-1}	5000, 78%	75% at 10 A g^{-1}	2
Ni,Co)Se_2/NiCo-LDH	170 mAh g^{-1} at 1 A g^{-1}	3000, 89%	71% at 20 A g^{-1}	3
NiCoSe-4	211 mAh g^{-1} at 1 A g^{-1}	5000, 90.31%	71.7% at 20 A g^{-1}	4
$CoSe_2$/$MoSe_2$-3-1	211.97 mAh g^{-1} at 1 A g^{-1}	2000, 94.2%	67.8% at 30 A g^{-1}	5
(GNR)/$Co_{0.85}Se$	76.4 mAh/g at 1 A g^{-1}	5000, 89%	73% at 10 A g^{-1}	6
$Ni_{1/2}Co_{1/2}Se_2$	166.1 mAh g^{-1} at 1 A g^{-1}	6000, 91.2%	75.1% at 20 A g^{-}	7
$Ni_{0.85}Se$	114.6 mAh g^{-1} at 1 A g^{-1}	5000, 73.9%	60.5% at 10 A g^{-1}	8
(Ni, Co)Se_2	106 mAh g^{-1} at 2 A g^{-1}	5000, 90.5%	75% at 10 A g	9
RB-NCS electrode	258.1 mAh g^{-1} at 1 A g^{-1}	14000, 92.2%	70.6% at 30 A g^{-1}	This work

References

1 C. Miao, X. Xiao, Y. Gong, K. Zhu, K. Cheng, K. Ye, J. Yan, D. Cao, G. Wang and P. Xu, Facile Synthesis of Metal–Organic Framework-Derived $CoSe_2$ Nanoparticles Embedded in the N-Doped Carbon Nanosheet Array and Application for Supercapacitors, *ACS Appl. Mater. Interfaces* 2020, **12**, 9365-9375.

2 H. Lei, J. Zhou, R. Zhao, H. Peng, Y. Xu, F. Wang, H. A. Hamouda, W. Zhang and G. Ma, Design and assembly of a novel asymmetric supercapacitor based on all-metal selenides electrodes, *Electrochim. Acta* 2020, **363**, 137206.

3 X. Li, H. Wu, C. Guan, A. M. Elshahawy, Y. Dong, S. J. Pennycook and J. Wang, $(Ni,Co)Se_2$/NiCo-LDH Core/Shell Structural Electrode with the Cactus-Like $(Ni,Co)Se_2$ Core for Asymmetric Supercapacitors, *Small* 2019, **15**, 1803895.

4 H. Liu, H. Guo, N. Wu, W. Yao, R. Xue, M. Wang and W. Yang, Rational design of nickel-cobalt selenides derived from multivariate bimetal metalorganic frameworks for high-performance asymmetric supercapacitor, *J. Alloys Compd*. 2021, **856**, 156535.

5 F. Ma, J. Lu, L. Pu, W. Wang and Y. Dai, Construction of hierarchical cobalt-molybdenum selenide hollow nanospheres architectures for high performance battery-supercapacitor hybrid devices, *J. Colloid Interface Sci*. 2020, **563**, 435-446.

6 Z. Chen, Y. Yang, Z. Ma, T. Zhu, L. Liu, J. Zheng and X. Gong, All-Solid-State Asymmetric Supercapacitors with Metal Selenides Electrodes and Ionic Conductive Composites Electrolytes, *Adv. Funct. Mater*. 2019, **29**, 1904182.

7 C. Miao, G. Xia, K. Zhu, K. Ye, Q. Wang, J. Yan, D. Cao, F. Gong and G. Wang, Enhanced supercapacitor performance of bimetallic metal selenides via controllable synergistic engineering of composition, *Electrochim. Acta* 2021, **370**, 137802.

8 S. Wu, Q. Hu, L. Wu, J. Li, H. Peng and Q. Yang, One-step solvothermal synthesis of nickel selenide nanoparticles as the electrode for high-performance supercapacitors, *J. Alloys Compd.* 2019, **784**, 347–353.

9 H. Lei, J. Zhou, R. Zhao, H. Peng, Y. Xu, F. Wang, H. A. Hamouda, W. Zhang and G. Ma, Design and assembly of a novel asymmetric supercapacitor based on all-metal selenides electrodes, *Electrochim. Acta* 2021, **363**, 137206.